Chemical Engineering Journal 166 (2011) 306–314

Contents lists available at ScienceDirect

Chemical Engineering Journal

journal homepage: www.elsevier.com/locate/cej

Two-dimensional computational fluid dynamics simulation of coal combustion in a circulating fluidized bed combustor

W. Zhou, C.S. Zhao*, L.B. Duan, C.R. Qu, X.P. Chen

School of Energy and Environment, Southeast University, Sipailou 2#, Nanjing 210096, China

ARTICLE INFO

Article history:
Received 5 May 2010
Received in revised form 2 September 2010
Accepted 10 September 2010

Keywords:
Coal combustion
Circulating fluidized bed
Computational fluid dynamic
Comprehensive model

ABSTRACT

A computational fluid dynamics (CFD) approach was applied to simulate the air-coal two-phase flow and combustion characteristics in a 50 kW circulating fluidized bed (CFB) combustor. Eulerian–Granular multiphase model with a drag coefficient correction based on the extended energy-minimization multi-scale (EMMS/matrix) model was used to study the gas–solid hydrodynamics. One energy conservation equation was applied to the mixture of gases and solids, considering heat conduction, heat convection and heat sources from chemical reactions. Reactions during coal combustion included moisture evaporation, dry coal devolatilization, volatile combustion, char combustion and char gasification. The model predicted the main features of the complex gas–solid flow, including the cluster formation of the solid phase along the walls, the flow structure of upward flow in the core and downward flow in the annular region. The voidage and temperature profiles in the furnace and the concentrations of gas components from the riser were validated with experimental data. Distributions of reaction rates in the riser were also obtained. This indicates a promising way to simulate the coal combustion in CFB to help understanding the combustion mechanism and designing new combustion technologies.

1. Introduction

During the past 20 years, circulating fluidized bed combustion technology has gained worldwide significant attention. With its well-known benefits of fuel flexibility, high combustion efficiency and low emissions, as well as easier temperature control during oxy-fuel combustion [1], CFB combustion technology becomes one of the most important developing directions for coal-fired boilers [2].

Mathematical modeling and simulation is helpful to better understanding of the combustion process and will be significant for CFB scale-up. The modeling researches in the end of the 20th century were reviewed and the furnace approach models were divided into three levels of sophistication [2]. Several models were developed and improved in the last decade. Huilin et al. established a 1.5-D steady state mathematical model for CFB coal combustion boilers [3] and the group investigated particle clustering effects on combustion and emission in a CFB riser via a 2-D CFD approach [4–8]. Adenz et al. [9,10] studied the carbon combustion efficiency and sulfur retention sub-models based on a previous model of fast bed CFB combustor. The model was applied for co-combustion of coal and biomass [10]. Gungor and Eskin established a 2-D CFB coal combustion model [11] with validation data from a pilot-scale 50 kW CFB combustor and an industrial-scale 160 MW CFB combustor. Sensitivity analysis of the operation parameters was carried out [12].

Macroscopic (semi-empirical) models for fluid dynamics of CFB units were presented with emphasis on applications for conditions relevant to industrial units such as fluidized-bed combustors [13]. A 3-D CFB model, initially developed in 1989, was modified to include the specific features under oxygen-enriched atmosphere [14,15]. Another 3-D CFB model [16–18], improved with semi-empirical models for concentration and temperature distributions, can predict the local conditions inside combustion chamber with arbitrary shapes and co-combustion of fuels.

CFD modeling of fluid dynamics has already reached a high level with two different approaches, the Eulerian–Eulerian approach and Eulerian–Lagrange approach. It was found that the multi-scale CFD approach in terms of EMMS/matrix seems to reach a mesh-independent solution of the sub-grid structure, and succeeds in predicting the axial profile and flow regime transitions [19,20]. Zhou et al. investigated the gas-particle turbulent flow in a CFB riser numerically by large eddy simulation (LES) coupled with Lagrangian approach [21]. While numerical modeling of reactive multiphase flows is still at an early stage [16]. CFD-based numerical model is used to simulate the gasification of coal [22] and biomass [23] inside an entrained flow gasifier. A 3-D numerical model was developed to simulate the coal gasification in a fluidized bed gasifier [24]. Jung and Gamwo [25] have developed the reaction kinetics model of the fuel reactor in a chemical looping

* Corresponding author. Tel.: +86 25 83793453; fax: +86 25 83793453.
E-mail address: cszhao@seu.edu.cn (C.S. Zhao).

1385-8947/$ – see front matter.
doi:10.1016/j.cej.2010.09.048

Nomenclature

C_{fix}	fixed carbon % by weight on air dried basis
C	mole concentration (kmol m^{-3})
d_p	particle diameter (m)
g	gravity (m s^{-2})
H	riser height (m)
h_m	mixture enthalpy (kJ kg^{-1})
J_i	diffusion flux of species i (kg m^{-3} s^{-1})
K	momentum exchange coefficient
k	reaction rate constant
k_m	mixture thermal conductivity (w m^{-1} s^{-1})
m	mass flow rate (kg m^{-3} s^{-1})
p	pressure (Pa)
R_i	mass flow rate of species i (kg m^{-3} s^{-1})
R	Universal gas constant (J kmol^{-1} K^{-1})
r	reaction rates (kmol m^{-3} s^{-1})
Re	Reynolds number
Sc	Schmidt number
Sh	Sherwood number
T	temperature (K)
t	time (s)
v	velocity (m s^{-1})
Y_i	mass fraction of species i

Greek letters

p	density (kg m^{-3})
ε_g	voidage
ε_s	solid volume fraction
τ	stress tensor (Pa)
Φ	mechanism factor
μ	viscosity, kg/m s

combustion process and implemented the kinetic model into a multiphase hydrodynamic model, MFIX, developed earlier at the National Energy Technology Laboratory.

Our recent thorough literature review shows that Euler–Granular CFD-based reaction models have not been adapted to circulating fluidized bed coal combustion processes in the open literature. In this study, an Euler–Granular model using the Kinetic Theory of Granular Flow (KTGF) and EMMS/Matrix correction was employed to simulate the hydrodynamics of gas–solid flow in a CFB riser, coupled with heat transfer and chemical reaction sub-models. The simulated voidage and temperature distribution and gas composition from the furnace outlet were validated against the experimental data from a 50 kW pilot CFB combustor at the Southeast University, China. Gas–solid flow patterns, gas velocities, particle velocities, composition profiles of gas product and other important characteristics in a circulating fluidized bed coal combustor were predicted.

2. Experimental

The experimental work reported here was carried out in a 50 kW pilot CFB combustor at the Southeast University, China. A detailed description of the experimental system can be found elsewhere [26]. Detailed dimensions of the CFB riser are shown in Fig. 1. The CFB riser column has a lower zone of 0.122 m and an upper zone of 0.150 m in I.D., with height of 0.800 m and 3.200 m, respectively. They are connected by a transition zone with the height of 0.200 m. The coal inlet is located on the left side of the riser at the height of 0.700 m above the primary oxidant inlet. The solid recycle inlet, the secondary oxidant inlet and furnace outlet are located on the right side at 0.200 m, 0.900 m and 4.085 m, respectively. To obtain the

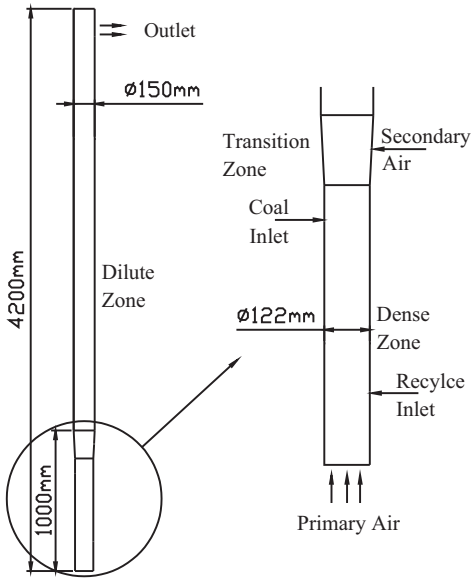

Fig. 1. Detail structure and dimensions of the CFB riser.

experimental temperature and voidage data, six thermal couples and six pressure taps are mounted at different elevations along the riser (H = 0.150, 0.700, 1.500, 2.900, 3.700, 4.000 m).

3. Model description

Based on CFD method, a comprehensive dynamic 2D planar model has been established to describe the coal combustion processes in the CFB riser. Parts of the important boundary and initial conditions used in the simulation are listed in Table 1. They are set in consistent with the experimental operation conditions to the largest extent.

3.1. Main assumptions

In order to eliminate the impact of the strong nonlinear characteristic of the model and ensure the good convergence and acceptable computational time, the comprehensive models are simplified as follows:

(i) The case simulated is assumed as two-dimensional with the furnace depth of 0.1 m. The widths of lower and upper zones in the 2-D simulation case are determined based on the corresponding cross-section area in the 3-D riser.
(ii) Simulated air flows (21% O_2/79% N_2) get into the CFB riser via the bottom or other inlets at uniform velocity distribution. Gas density follows the incompressible ideal gas law.
(iii) Particles are assumed isothermal, inelastic and smooth spheres.
(iv) Small interaction forces such as lift force, thermophoretic force, Brownian force and virtual mass force are neglected. Energy transfer due to pressure stress work, viscous dissipation and species diffusion are not considered.

3.2. Governing equations

The mass and momentum conservation equations are applied to each phase (gas and solid). Those for gas phase are given as Eqs. (1) and (2). For the interphase momentum exchange coefficient K_{sg}, Wen and Yu drag model corrected by EMMS/matrix coefficient is compared with the Gidaspow model [27]. The EMMS/matrix correction is obtained from EMMS software supplied by Institute of

Table 1
Parts of parameters used in simulations.

Parameters	Value	Parameters	Value
Real density of char particles	1280 kg/m^3	Primary air ratio	0.7
Real density of ash particles	2400 kg/m^3	Primary air temperature	400 K
Particle diameter	0.35 mm	Secondary air temperature	298 K
Coal feed rate	8 kg/h	Heat loss through dilute zone wall	20%
Inlet coal temperature	298 K	Boundary condition in the dense zone	Adiabatic
Excess air coefficient	1.2	Initial furnace temperature	1123 K

Table 2
Ultimate and proximate analysis of Xuzhou bituminous coal.

Sample	Ultimate analysis/wt%					LHV	Proximate analysis/wt%			
	C_{ad}	H_{ad}	O_{ad}	N_{ad}	S_{ad}	MJ kg^{-1}	FC_{ad}	V_{ad}	A_{ad}	M_{ad}
Xuzhou coal	58.97	3.65	7.30	0.67	1.76	23.54	47.33	25.02	25.55	2.10

Process Engineering, Chinese Academy of Sciences. Detail descriptions of the model can be found in the literatures [28,29]. Meaning of other symbols can be found in the nomenclature. The standard κ–ε model is adopted to simulate the gas phase turbulence and KTGF for the solid phase [30]. The species conservation equations are solved for individual species, as given by Eq. (3) for gas species. As part of the comprehensive model, the complicated processes of chemical reactions are considered by setting the source terms of mass, momentum and/or species transport equations when the reactants are consumed and the products are created.

$$\frac{\partial}{\partial t}(\varepsilon_g\rho_g) + \nabla\cdot(\varepsilon_g\rho_g\vec{\upsilon}_g) = \dot{m}_{sg} \tag{1}$$

$$\frac{\partial}{\partial t}(\varepsilon_g\rho_g\vec{\upsilon}_g) + \nabla\cdot(\varepsilon_g\rho_g\vec{\upsilon}_g\vec{\upsilon}_g) = -\varepsilon_g\nabla p + \nabla\cdot\overline{\overline{\tau_g}} + \varepsilon_g\rho_g g + K_{sg}(\vec{\upsilon}_s - \vec{\upsilon}_g) + \dot{m}_{sg}\vec{\upsilon}_s \tag{2}$$

$$\frac{\partial}{\partial t}(\varepsilon_g\rho_g Y_i) + \nabla\cdot(\varepsilon_g\rho_g\vec{\upsilon}_g Y_i) = -\nabla\cdot\vec{J}_i + R_i \tag{3}$$

However, as the mechanism of heterogeneous reaction provided by FLUENT software, heat generated during char combustion is absolutely absorbed by the gas phase at first and then is partly transferred to the solid phase through interphase heat convection and radiation. That poses a great challenge to the numerical simulation of interphase heat transfer. In this study, considering the excellent performance of interphase heat transfer in the circulating fluidized bed and large amount of inert materials in the solid phase, the temperature differences between phases at the same location are ignored for simplification. Therefore, gases and solids are treated as one mixed phase (mixture) and one conservation equation of mixture enthalpy h_m is applied as

$$\frac{\partial}{\partial t}(\rho_m h_m) + \nabla\cdot(\rho_m\vec{\upsilon}_m h_m) = \nabla\cdot(k_m\nabla T_m) + S_m \tag{4}$$

where mixture density ρ_m, mixture velocity $\vec{\upsilon}_m$ and mixture thermal conductivity k_m are calculated according to $\rho_m = \sum_p \varepsilon_p\rho_p$, $\rho_m\vec{\upsilon}_m = \sum_p \varepsilon_p\rho_p\vec{\upsilon}_p$, and $k_m = \sum_p \varepsilon_p k_p$, respectively. ε_p is volume fraction of the phase p. S_m characterizes the heat sources from chemical reactions. This method is proved to be dependable and time saving in numerical modeling, with reasonable simulation results.

3.3. Chemical reactions

The solid phase consists of 4 species (dry coal $C_{4.914}H_{3.650}O_{0.456}$, moisture H_2O, char C and ash) and the gas phase consists of 8 species (methane CH_4, oxygen O_2, carbon monoxide CO, carbon dioxide CO_2, water vapor H_2O, hydrogen H_2, tar $CH_{2.596}O_{0.158}$ and nitrogen N_2). The equivalent formula of the dry coal and tar is deduced combining with the proximate and ultimate analysis of the coal tested [31], as displayed in Table 2. In the present model, reactions related with sulfur or nitrogen are not taken into account and they are considered passing directly to ash, but they are expected to be considered in the future work. The simulated processes during coal combustion include moisture evaporation, coal devolatilization, volatile combustion, char combustion and char gasification.

In most coal combustion modeling researches, moisture evaporation process was omitted or assumed to happen promptly once the coal was fed into the furnace. It is assumed in this paper that the moisture evaporation rate is 10 times as high as the devolatilization rate. The dry coal is consumed according to (R1). The volatile consists of CH_4, CO, H_2O, CO_2, H_2 and tar, whose fraction composi-

Table 3
Rates for the chemical reactions.

	Reaction rate r/kmol m^{-3} s^{-1}	Reaction rate constant k
(R1)	$r_1 = k_1 C_{rawc}$	$k_1 = 4.136\times10^4\exp(-0.73\times10^8/RT)$ [33]
(R2)	$r_2 = k_2 C_{O_2}^{0.8} C_{CH_4}^{0.7}$	$k_2 = 5.0122\times10^{11}\exp(-2.0085\times10^8/RT)$ [a] [34]
(R3)	$r_3 = k_3 Y_{CO} Y_{H_2O}^{0.5} \frac{17.5Y_{H_2O}}{1+24Y_{H_2O}} \left(\frac{p}{RT}\right)^{1.8}$	$k_3 = 3.25\times10^{10}\exp(-1.255\times10^8/RT)$ [11]
(R4)	$r_4 = k_4 C_{H_2}^{1.5} C_{O_2}$	$k_4 = 1.03\times10^{14}T^{-1.5}\exp(-0.284\times10^8/RT)$ [a] [34]
(R5)	$r_5 = k_5 C_{tar} C_{O_2}$	$k_5 = 3.80\times10^7\exp(-0.555\times10^8/RT)$ [35]
(R6)	$r_6 = \frac{6(1-\varepsilon)\rho_s Y_{char}}{d_p\rho_c}\cdot k_c C_{O_2}$ [b] $k_c = \frac{RT/w_c}{(1/\phi k_d)+(1/k_2)}$	$k_6 = 8910\exp(-1.4974\times10^8/RT)$, $k_d = ShD_g w_c/d_p RT_g$ [b] $Sh = 2\varepsilon + 0.69(Re/\varepsilon)^{1/2}Sc^{1/3}$, $Re = ud_p\rho_g/\mu_g$, $Sc = \mu_g/\rho_g D_g$ $D_g(T,p) = D_g(T_0,p_0)[T/T_0]^{1.75}[p_0/p]$ $D_g(T_0,p_0) = 3.13\times10^{-4}$ m^2/s, $T_0 = 1500$ K, $p_0 = 101{,}325$ Pa [11,36]
(R7)	$r_7 = \frac{6(1-\varepsilon)\rho_s Y_{char}}{d_p\rho_c}\cdot k_7 C_{CO_2}$	$k_7 = 4.1\times10^6\exp(-29787/T)$ [11]

[a] Unit of molar concentration C in this paper is kmol m^{-3} and this leads to different coefficients with the references.
[b] Unit of universal gas component R in the two formulas is kJ kmol^{-1} K^{-1}.

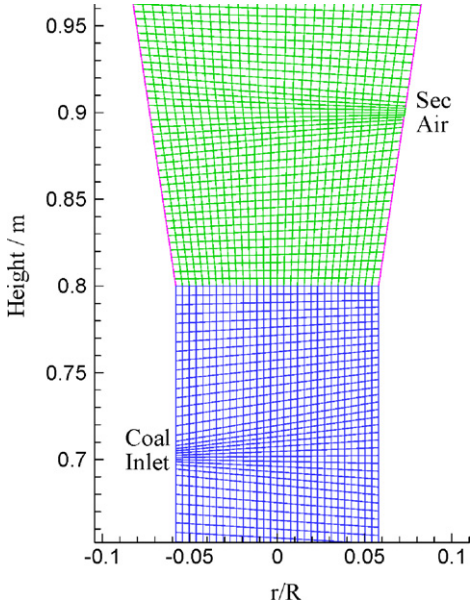

Fig. 2. Mesh refinement near the inlets.

tions are determined based on the Loison and Chauvin model [11]. To get the real data of volatile compositions, an experiment was performed on the tube furnace for the bituminous coal pyrolysis. The similar ratio of CH_4/CO was obtained between experimental and Loison and Chauvin model. Combustion of volatiles takes place according to the homogeneous reactions ((R2)–(R5)). The char is consumed according to heterogeneous combustion (R6) and gasification (R7) reactions.

$$1\,\text{kg drycoal} \rightarrow Y_c\,\text{kg char} + Y_v\,\text{kg volatile} + (1 - Y_c - Y_v)\,\text{kg ash} \quad \text{(R1)}$$

$$CH_4 + \tfrac{3}{2}O_2 \rightarrow CO + 2H_2O \quad \text{(R2)}$$

$$CO + \tfrac{1}{2}O_2 \rightarrow CO_2 \quad \text{(R3)}$$

$$H_2 + \tfrac{1}{2}O_2 \rightarrow H_2O \quad \text{(R4)}$$

$$CH_{2.596}O_{0.158} + 1.570O_2 \rightarrow CO_2 + 1.298H_2O \quad \text{(R5)}$$

$$C + \frac{1}{\Phi}O_2 \rightarrow \left(2 - \frac{2}{\Phi}\right)CO + \left(\frac{2}{\Phi} - 1\right)CO_2 \quad \text{(R6)}$$

$$C + CO_2 \rightarrow 2CO \quad \text{(R7)}$$

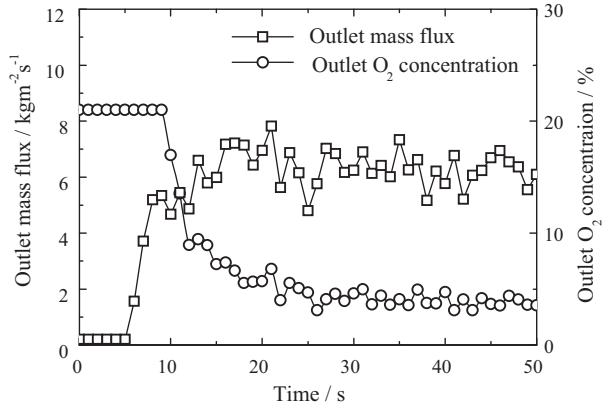

Fig. 3. Changes over time of monitored variables through the outlet during simulation.

Φ is a mechanism factor which is determined by particle diameter and combustion temperature, as usually adopted by literatures [11,16,32].

$$\Phi = \begin{cases} \dfrac{2p+2}{p+2} & d_c < 0.05\,\text{mm} \\ \dfrac{2p+2-(p/0.095)(100d_c-0.005)}{p+2} & 0.05\,\text{mm} \le d_c \le 1.0\,\text{mm} \\ 1.0 & d_c > 1.0\,\text{mm} \end{cases}$$

where $p = 2500\exp[-5.19 \times 10^4/RT_s]$.

The rates of coal devolatilization and volatile combustion are controlled by Arrhenius law, and the pre-exponential factor and activation energy are obtained from the Fu-Zhang general pyrolysis model [33] and other literatures [11,34,35], respectively. According to Field et al. [36], the char combustion rate is described by both the chemical kinetic reaction rate and the diffusion rate of oxygen to the particle surface and internal pores, which is widely used in fluidized bed combustion. Detailed formulas are listed in Table 3.

3.4. Numerical considerations

The bed is initially filled with ash particles with static height of 0.4 m, where the volume fraction of the solids is 0.55. The maximum particle packing is limited to 0.63. The no-slip wall condition is used for the gas phase and partial-slip boundary condition for the solid phase. The particle–particle restitution and specularity coefficient are set as 0.9 and 0.001, respectively. The specific heat capacity of each gas species is calculated as a piecewise-linear function of temperature and viscosity as power law. Physical parameters of the gas and solid mixtures obey the volume/mass-weighted-mixing law.

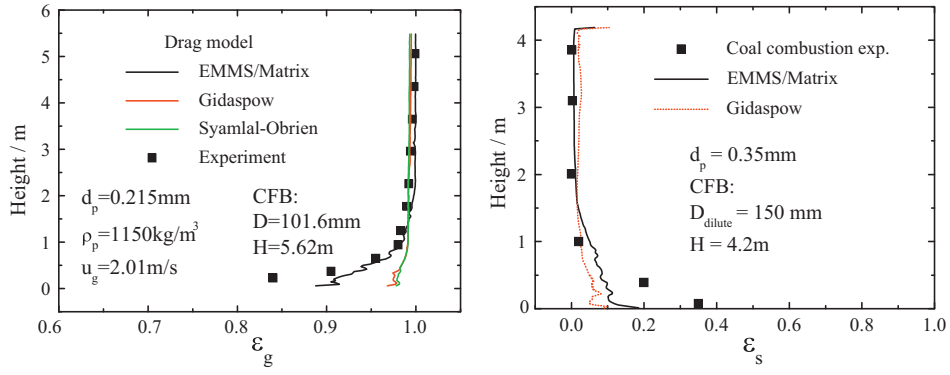

(a) CFB in the reference (b) CFB in this paper

Fig. 4. Comparison of time-averaged voidage distributions for two CFBs based on different drag models.

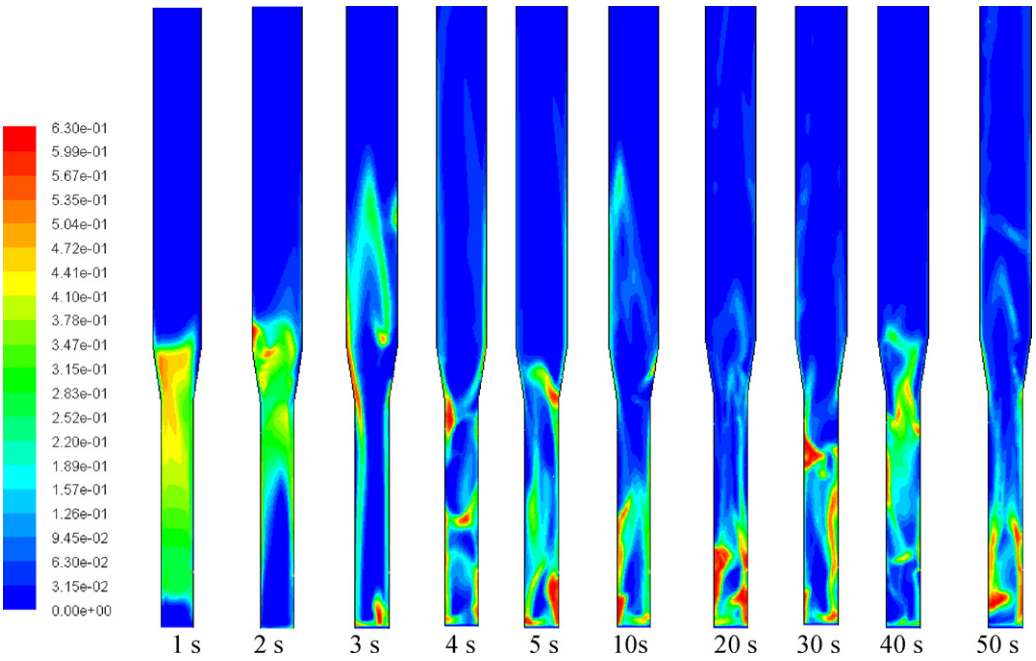

Fig. 5. Time series of the gas-particle flow in the lower part of the riser in the from of solid volume fraction.

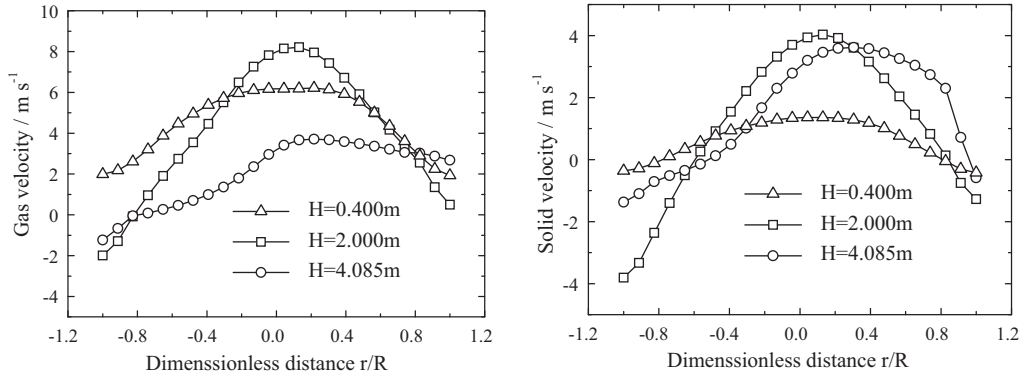

Fig. 6. Radial profiles time-averaged Y velocity for gas and solid phases.

During the simulation, mass fractions of the solid species through the solid recycle inlet are set the same as the outlet conditions. To maintain constant bed inventory, mass flow rate of the recycled solid is adjusted at real time combining the mass flow

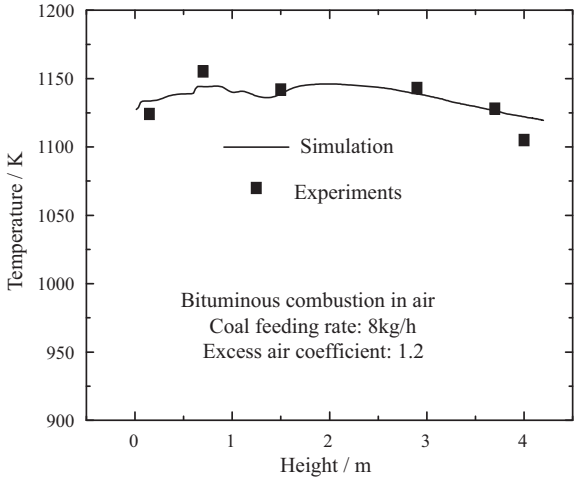

Fig. 7. Temperature profile along the furnace.

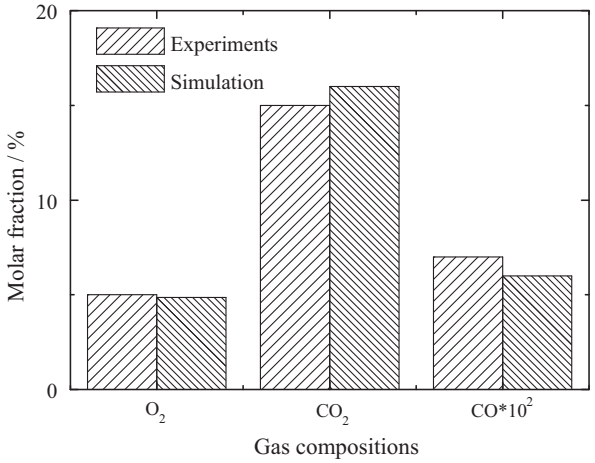

Fig. 8. Gas compositions from the outlet.

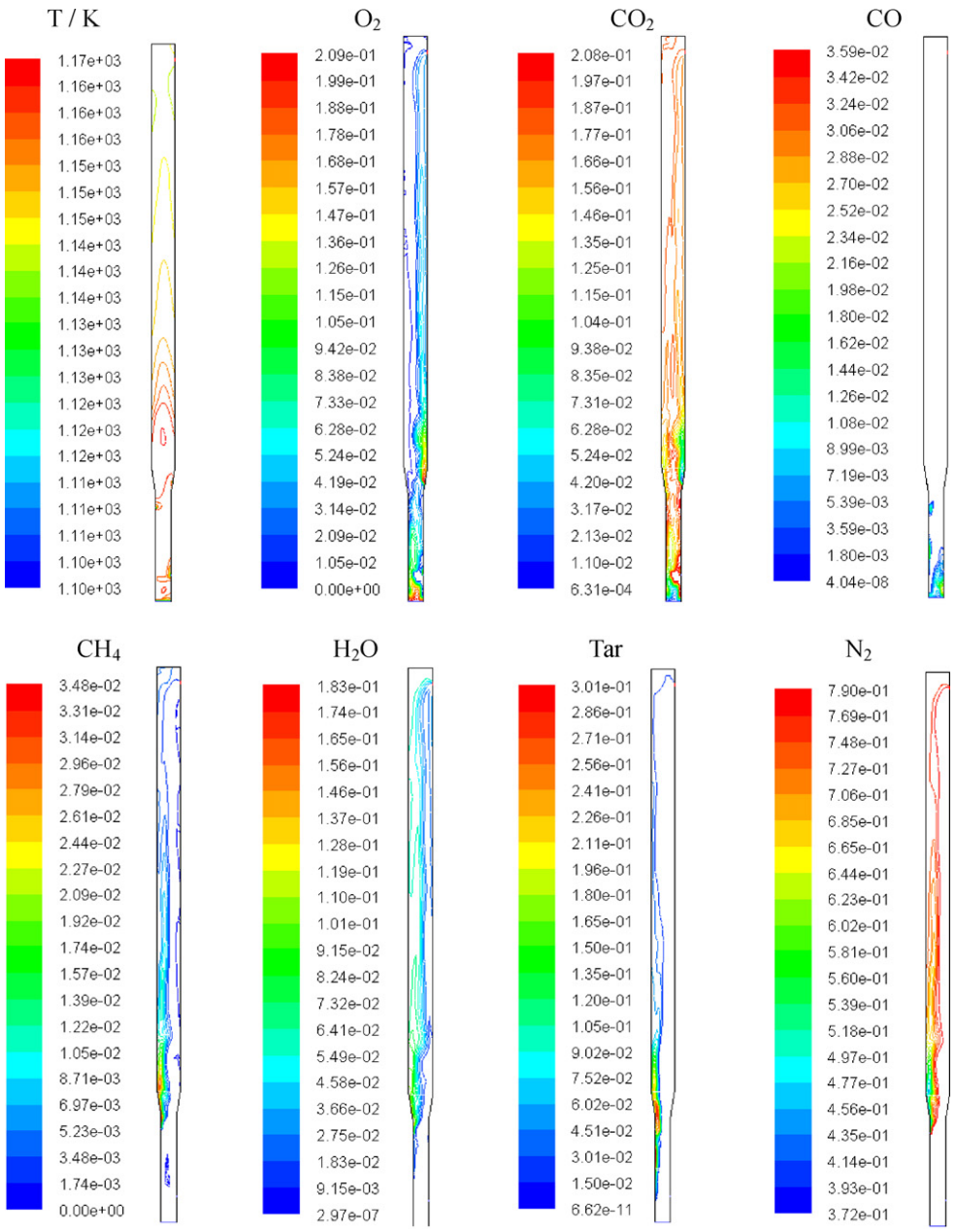

Fig. 9. Contours of the predicted temperature and gas composition distributions.

rate of feeding coal and outlet solid. According to experimental measured data, temperature of recycled solid is set to make sure that 30% of the thermal input is released along the dipleg and the loopseal.

After mesh independent analysis, 5 mm × 5 mm grids are applied in the dense and transition zones and 8 mm × 15 mm in the dilute zone. As shown in Fig. 2, mesh refinements near the inlets are applied and the total mesh number is nearly 8500. The time step is set as 1×10^{-4}. For the first 10 s, gas–ash fluidization is simulated at the temperature of 1123 K without coal feeding, and then coal is continuously fed into the furnace at 8 kg/h. The simulation was conducted for 50 s and it cost nearly 20 days on an Intel w5580 workstation. Time-averaged distributions of flow and combustion characteristic variables were computed for the period from 30 s to 50 s.

4. Results and discussions

Fig. 3 shows the changes over time of mixture mass flux through the furnace outlet and O_2 concentration in the flue gas from the outlet during simulation. They are monitored for the judgement of steady-state coal combustion processes. It indicates that the time averaged variables computed from 30 s to 50 s are representative in description of primary characteristics for the simulated case.

4.1. Flow characteristics

Before this comprehensive modeling research, the validation of hydrodynamic model was carried out through the comparison with the cold experimental data on a CFB from Ref. [37]. The dimensions

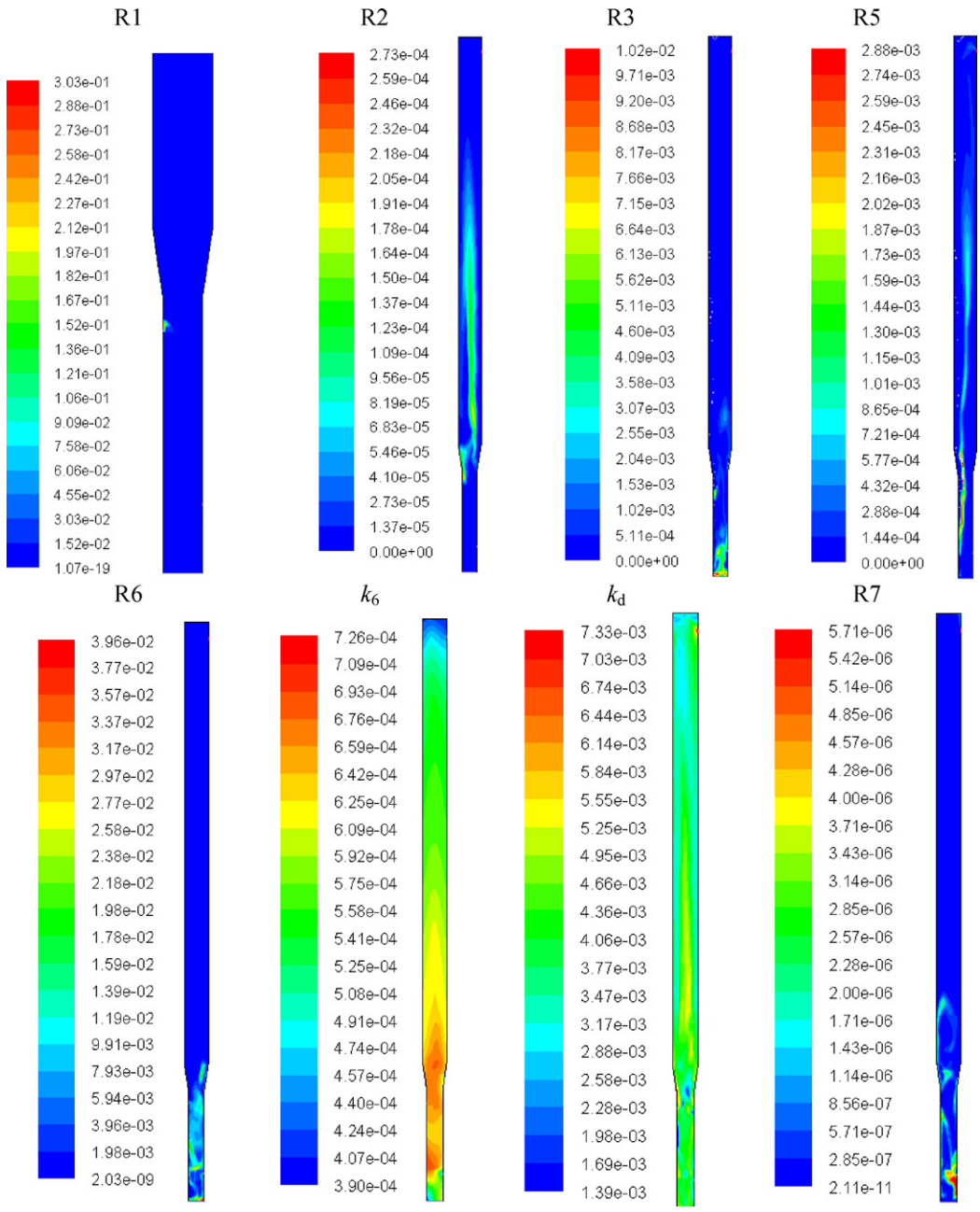

Fig. 10. Contours of reaction rates.

of the CFB were similar to those introduced in this paper except the smooth exit geometry. The experimental operation conditions were described in detail [37] and the simulation conditions were set accordingly. Fig. 4(a) shows the comparison of time-averaged voidage distributions based on different drag models. It indicates that the model with EMMS/Matrix drag correction predicts more obvious dense zone and the simulation results are more close to the experimental data. The trends are similar with the simulation results obtained from other researches [38]. As shown in Fig. 4(b), the consistent results are also concluded from the simulations of gas–solid flow in our hot CFB. The experimental solid volume fractions are calculated from the pressure distribution. The gap between EMMS/Matrix simulation and experiments is due to the assumption of average diameter of the bed material. The difference of the voidage distribution between these two CFB exists near the top of the furnace. Fig. 4(b) shows that the abrupt T-type outlet geometry leads to a gathering of particles in the top zone. The hydrodynamic model with EMMS/Matrix drag correction was applied in following simulations.

For the operation condition listed in Table 3, a time series of the computed flow patterns in the form of solid volume fraction are illustrated in Fig. 5. A typical turbulent fluidization pattern is observed in the lower zone of the riser. In the upper zone, taking on horseshoe-shaped clusters, the packets of particles form, grow, change their shapes, break up and form again ceaselessly. Fig. 6 shows radial profiles of time-averaged axial solid velocity and axial gas velocity at three different heights. $H = 0.400$ m, $H = 2.100$ m and $H = 4.085$ m are located at the middle of dense zone, the middle of the furnace length and the outlet height, respectively. The clusters of particles accumulate near the wall until they become sufficiently heavy that they could not be carried by the gas, forming a core-annular flow structure with a dilute rising core and a

dense descending annular region. The gas is also detected moving downward near some wall region showing the strong effect of downward solids. The maximum axial velocity is detected in the core for both solid and gas in most of the region in the riser. While at the outlet level, higher gas and solid velocities on the right side appear, which reveals the impact of outlet geometry. In general, those figures show that the model is capable of predicting the nearly axisymmetrical flow patterns for the case, despite the unsymmetrical configuration of the inlet and outlet geometry [39].

4.2. Temperature and gas composition profiles

The simulated axial distributions of cross-section averaged mixture temperature at the moment of 50 s are displayed in Fig. 7. Experimental data are used to validate the model and a good agreement is achieved. The primary air temperature increases dramatically to the bed temperature level near the air distributor. A peak value is detected near the coal feeding height because of the dramatic volatile combustion and then it decreases in some sort due to the cold secondary air injection. Simultaneously, the secondary air supplies sufficient oxygen for volatile and char combustion and the exothermic reactions lead to a temperature rise in the upper zone. Then temperature decreases gradually because of heat release in the dilute zone through the furnace wall.

Fig. 8 shows the comparisons between the predicted results and the experimental data of gas concentrations from the outlet. The form of area-averaged molar fraction is adopted. The results of these main gas components show a good agreement with experiments. The maximum error is <15%. It implies that the present 2D numerical simulations are reasonable and the validity of the present model is verified.

Contours of the predicted temperature and gas composition distributions in the riser at the moment of 50 s are shown in Fig. 9. The first figure reveals a relatively uniform gas temperature in the radial direction with a difference of about 50 K along the CFB combustor. Gas compositions are shown in the form of molar fraction. The O_2 concentration decreases along the combustor with a sudden increase near the secondary air inlet, while CO_2 shows the opposite tendency. The very high concentrations of volatiles (CH_4, CO, H_2O, H_2 and tar) appear near the coal feeding point due to the devolatilization and then the concentrations drop down gradually because of combustion reaction. With the devolatilization model mentioned in Section 3.3, the predicted tar concentration is much higher than that of other volatiles. Similar to CH_4 profile, H_2 profile is not displayed here. Low concentrations of O_2 and N_2 appear near the coal feeding point correspondingly. A certain amount of CO is observed in the dense zone since it is produced mostly through coal combustion, while dry coal devolatilization, CH_4 combustion and coal gasification contribute a little. Large amount of volatiles are also observed in the lower part of the dilute zone.

4.3. Reaction rates

Fig. 10 illustrates the rates of heterogeneous and homogenous reactions referred to in this CFB combustion model. It can be observed that once the raw coal enters the riser, it releases the volatiles quickly with the devolatilization rate 10–1000 times larger than other reaction rates. Rates of homogeneous reactions ((R2)–(R5)) show obviously that the volatile products combust largely in the upper dilute zone in circulating fluidized bed. And the assumption of complete volatile combustion in the dense zone from some modeling researches may not be accurate, especially for this bituminous coal with high volatile content. As can be seen from Figs. 9 and 10, the temperature rise in the dilute zone is mostly due to the heat release from volatile combustion.

Heterogeneous char combustion reaction (R6) mainly takes place in the lower dense zone and the transition zone. As mentioned in Section 3.3 and Table 3, the chemical kinetic reaction rate k_6 and the oxygen diffusion rate k_d are integrated to describe the char combustion rate. k_6 is a function of temperature and k_d is influenced by both the gas–solid hydrodynamics and the temperature distribution. Fig. 10 shows that k_d is 10 times larger than k_6, which reveals that the char combustion rate under this simulated condition is controlled by the kinetic reaction rate. For coal combustion in air, char gasification (R7) can be ignored for its much lower reaction rate. But the influence of gasification is one of our interests for the oxy-fuel combustion, which will be executed next in detail using this comprehensive model.

The combustion fraction in the CFB combustor can be analyzed by statistical calculation of reaction rate. For the moment of 50 s, the molar fraction of gas combustion in the upper dilute zone achieves 0.56 and the char combustion fraction in the dense zone is about 0.72.

5. Conclusions

A comprehensive CFD model based on Two Fluid Model using KTGF was developed to simulate the coal combustion process in a CFB riser. Coal combustion characteristics in air were studied. The model consists of hydrodynamic model, heat transfer model and mass transfer model including homogeneous and heterogeneous reactions. The results show reasonable distributions of temperature, solid volume fraction, solid velocity, gas velocity and gas compositions in the combustor and the results are in good agreement with the experimental data. Using this comprehensive model, detailed information such as concentration and chemical reaction rate profiles are easy to obtain. This proposes a promising way for studying the coal combustion in CFB, especially for new technologies such as oxy-fuel combustion.

Acknowledgement

Financial supports of this work by the National Key Program of Basic research of China (2006CB705806) and National Key Technology R&D Program of China (2006BAA03B02) are gratefully acknowledged.

References

[1] T. Czakiert, Z. Bis, W. Muskala, W. Nowak, Fuel conversion from oxy-fuel combustion in a circulating fluidized bed, Fuel Process. Technol. 87 (2006) 531–538.
[2] P. Basu, Combustion of coal in circulating fluidized-bed boilers: a review, Chem. Eng. Sci. 54 (1999) 5547–5557.
[3] L. Huilin, Z. Guangbo, B. Rushan, C. Yongjin, D. Gidaspow, A coal combustion model for circulating fluidized bed boilers, Fuel 79 (2000) 165–172.
[4] S.Y. Wang, L.J. Yin, H.L. Lu, J.M. Ding, L. Yu, L. Xiang, Numerical analysis of particle clustering effects on desulphurization and NO emission in a circulating fluidized bed combustor, Fuel 87 (2008) 870–877.
[5] H.L. Lu, S.Y. Wang, Y.R. He, J.M. Ding, G.D. Liu, Z.H. Hao, Numerical simulation of flow behavior of particles and clusters in riser using two granular temperatures, Powder Technol. 182 (2008) 282–293.
[6] S. Wang, H. Lu, Y. Zhao, R. Mostofi, K.H. Young, L. Yin, Numerical study of coal particle cluster combustion under quiescent conditions, Chem. Eng. Sci. 62 (2007) 4336–4347.
[7] Z. Yunhau, L. Huilin, H. Yurong, J. Ding, Y. Lijie, Numerical prediction of combustion of carbon particle clusters in a circulating fluidized bed riser, Chem. Eng. J. 118 (2006) 1–10.
[8] X.J. Liu, L. Li, Numerical studies on the combustion properties of char particle clusters, Int. J. Heat Mass Trans. 52 (2009) 4785–4795.
[9] J. Adanez, P. Gayan, G. Grasa, L.F. de Diego, L. Armesto, A. Cabanillas, Circulating fluidized bed combustion in the turbulent regime: modelling of carbon combustion efficiency and sulphur retention, Fuel 80 (2001) 1405–1414.
[10] P. Gayan, J. Adanez, L.F. de Diego, L.F. Garcia, A. Cabanillas, A. Bahillo, M. Aho, K. Veijonen, Circulating fluidised bed co-combustion of coal and biomass, Fuel 83 (2004) 277–286.
[11] A. Gungor, Two-dimensional biomass combustion modeling of CFB, Fuel 87 (2008) 1453–1468.

[12] A. Gungor, Analysis of combustion efficiency in CFB coal combustors, Fuel 87 (2008) 1083–1095.
[13] D. Pallar, F. Johnsson, Macroscopic modelling of fluid dynamics in large-scale circulating fluidized beds, Prog. Energy Combust. 32 (2006) 539–569.
[14] J. Krzywanski, T. Czakiert, W. Muskala, R. Sekret, W. Nowak, Modeling of solid fuels combustion in oxygen-enriched atmosphere in circulating fluidized bed boiler: part 1. The mathematical model of fuel combustion in oxygen-enriched cfb environment, Fuel Process. Technol. 91 (2010) 290–295.
[15] J. Krzywanski, T. Czakiert, W. Muskala, R. Sekret, W. Nowak, Modeling of solid fuel combustion in oxygen-enriched atmosphere in circulating fluidized bed boiler: part 2. Numerical simulations of heat transfer and gaseous pollutant emissions associated with coal combustion in O_2/CO_2 and O_2/N_2 atmospheres enriched with oxygen under circulating fluidized bed conditions, Fuel Process. Technol. 91 (2010) 364–368.
[16] R. Wischnewski, L. Ratschow, E.U. Hartge, J. Werther, Reactive gas–solids flows in large volumes – 3d modeling of industrial circulating fluidized bed combustors, Particuology 8 (2010) 67–77.
[17] J. Werther, E.U. Hartge, L. Ratschow, R. Wischnewski, Simulation-supported measurements in large circulating fluidized bed combustors, Particuology 7 (2009) 324–331.
[18] T. Knoebig, K. Luecke, J. Werther, Mixing and reaction in the circulating fluidized bed – a three-dimensional combustor model, Chem. Eng. Sci. 54 (1999) 2151–2160.
[19] W. Wang, B. Lu, N. Zhang, Z. Shi, J. Li, A review of multiscale CFD for gas–solid CFB modeling, Int. J. Multiphas. Flow 36 (2010) 109–118.
[20] N. Zhang, B. Lu, W. Wang, J. Li, Virtual experimentation through 3d full-loop simulation of a circulating fluidized bed, Particuology 6 (2008) 529–539.
[21] H. Zhou, G. Flamant, D. Gauthier, Modelling of the turbulent gas-particle flow structure in a two-dimensional circulating fluidized bed riser, Chem. Eng. Sci. 62 (2007) 269–280.
[22] W. Vicente, S. Ochoa, J. Aguill, E. Barrios, An Eulerian model for the simulation of an entrained flow coal gasifier, Appl. Therm. Eng. 23 (2003) 1993–2008.
[23] D.F. Fletcher, B.S. Haynes, F.C. Christo, S.D. Joseph, A CFD based combustion model of an entrained flow biomass gasifier, Appl. Math. Model. 24 (2000) 165–182.
[24] X. Wang, B. Jin, W. Zhong, Three-dimensional simulation of fluidized bed coal gasification, Chem. Eng. Process.: Process Intens. 48 (2009) 695–705.
[25] J. Jung, I.K. Gamwo, Multiphase CFD-based models for chemical looping combustion process: fuel reactor modeling, Powder Technol. 183 (2008) 401–409.
[26] W. Zhou, C.S. Zhao, L.B. Duan, C.R. Qu, J.Y. Lu, X.P. Chen, Numerical simulation on hydrodynamics and combustion in a circulating fluidized bed under O_2/CO_2 and air atmospheres, in: Presented at 20th International Conference on Fluidized Bed Combustion, May 18, 2009 – May 21, 2009, Xian, China, 2009.
[27] W. Du, X. Bao, J. Xu, W. Wei, Computational fluid dynamics (CFD) modeling of spouted bed: assessment of drag coefficient correlations, Chem. Eng. Sci. 61 (2006) 1401–1420.
[28] W. Wang, J. Li, Simulation of gas–solid two-phase flow by a multi-scale CFD approach – of the EMMS model to the sub-grid level, Chem. Eng. Sci. 62 (2007) 208–231.
[29] B. Lu, W. Wang, J. Li, Searching for a mesh-independent sub-grid model for CFD simulation of gas–solid riser flows, Chem. Eng. Sci. 64 (2009) 3437–3447.
[30] D. Gidaspow, J. Jung, R.K. Singh, Hydrodynamics of fluidization using kinetic theory: an emerging paradigm: 2002 flour-daniel lecture, Powder Technol. 148 (2004) 123–141.
[31] L. Duan, C. Zhao, W. Zhou, C. Liang, X. Chen, Sulfur evolution from coal combustion in O_2/CO_2 mixture, J. Anal. Appl. Pyrol. 86 (2009) 269–273.
[32] I.B. Ross, J.F. Davidson, The combustion of carbon particles in a fluidized-bed, Trans. Inst. Chem. Eng. 60 (1982) 109–114.
[33] W.B. Fu, Y.P. Zhang, H.Q. Han, D.F. Wang, A general-model of pulverized coal devolatilization, Fuel 68 (1989) 505–510.
[34] E. Desroches-Ducarne, J.C. Dolignier, E. Marty, G. Martin, L. Delfosse, Modelling of gaseous pollutants emissions in circulating fluidized bed combustion of municipal refuse, Fuel 77 (1998) 1399–1410.
[35] J.M. Heikkinen, B.C. Venneker, G.D. Nola, W.D. Jong, H. Spliethoff, CFD simulation and experimental validation of co-combustion of chicken litter and MBM with pulverized coal in a flow reactor, Fuel Process. Technol. 89 (2008) 874–889.
[36] M.A. Field, D.M. Gill, B.B. Morgan, P.G.W. Hawskley, Combustion of Pulverized Coal, BCURA, Leatherhead, England, 1987.
[37] M. Das, A. Bandyopadhyay, B.C. Meikap, R.K. Saha, Axial voidage profiles and identification of flow regimes in the riser of a circulating fluidized bed, Chem. Eng. J. 145 (2008) 249–258.
[38] J.W. Wang, W. Ge, J.H. Li, Eulerian simulation of heterogeneous gas–solid flows in CFB risers: EMMS-based sub-grid scale model with a revised cluster description, Chem. Eng. Sci. 63 (2008) 1553–1571.
[39] A. Almuttahar, F. Taghipour, Computational fluid dynamics of high density circulating fluidized bed riser: study of modeling parameters, Powder Technol. 185 (2008) 11–23.